ASTEROID IMPACTS ON THE OCEAN AND THEIR SHORT-TERM CONSEQUENCES: A PORTUGUESE CASE STUDY

R.H.Morais,[a] *L.F.F.M.Santos,*[ab] *A.R.R.Silva*[a]*, Rui Melicio*[cd]

[a]LAETA-AEROG, Universidade da Beira Interior, 6200-358 Covilhã, Portugal
[b]ISEC Lisboa, 1750-142 Lisboa, Portugal
[c]LAETA-IDMEC, Instituto Superior Técnico, Universidade de Lisboa, 1049-001 Lisboa, Portugal
[d]ICT, Universidade de Évora, 7002-554 Évora, Portugal

ABSTRACT

Any location on Earth might be considered a subject to an asteroid impact because, as previous studies show, they are a proven global threat. the consequences of a collision could be catastrophic, even though such events are rare to occur in a person's lifetime. Tsunami waves can constitute the greatest threat as the Earth's surface is mostly water, making the probability of a water impact greater than a ground impact. This work expands the knowledge about asteroid impacts on the ocean and their short-term regional consequences. Three asteroids were assumed to impact the Earth: (1) the 2015 JJ asteroid with a 130 m diameter, (2) the 2020 FA_5 asteroid with a 210 m diameter, and (3) the Apophis asteroid, a 370 m wide asteroid. We evaluated the consequences of all impacts, at a 45 degree angle, for a specific case study, where the chosen impact location was the midpoint between Portugal's mainland, Azores, and Madeira Islands. The cratering process, overpressure, induced thermal radiation, and tsunami waves were assessed, along with the global effects. The overpressure mainly causes structural damage. The thermal radiation has too short a range to reach the studied localities. The tsunami is undoubtedly the most far-reaching and threatening effect of an asteroid impact in the ocean.

Index Terms— 2015 JJ, 2020 FA_5, Apophis, impact effects, vulnerabilities, casualties

1. INTRODUCTION

Collisions with hazardous asteroids are not a frequent occurrence. Nevertheless, asteroids have been impacting the Earth since its creation and they can still pose a threat to populations, reinforcing the relevance of this study.

The asteroid 2015 JJ is a Near-Earth Object (NEO) with an estimated diameter of 130 meters, and was first observed in May 2003. It belongs to the Apollo family [1] and has 1 potential impacts with Earth in 2111. Its cumulative impact probability is 2.1×10^{-5} which corresponds to a value of -3.57 on the Palermo Scale [2]. The estimated velocity at atmospheric entry is 15.45 km.s^{-1}, while the mass density is 2.6 g.cm^3. The 2020 FA_5 asteroid was observed between February 19 and March 25 in 2020 and is considered a NEO and a Potentially Hazardous Asteroid (PHA). The asteroid belongs to the Apollo group [3] and has an estimated diameter of 210 m, and a mass density of 2.6 g.cm^3. The asteroid has 2 potential impacts with Earth in 2110 with an impact probability of 2.7×10^{-6}, corresponding to a Palermo Scale value of -3.53 [4]. The estimated velocity at atmospheric entry is 29.70 km.s^{-1}.

The Apophis asteroid has an estimated 370 m diameter [5, 6] and was first discovered in 2004. Given the initial observation, a high probability of impact was predicted in 2029, reaching an unprecedented value of four on the Torino scale [7] – it is one of the best-known asteroids. This 2029 impact possibility was disregarded with updated observations [8], nevertheless, it was still considered a 2036 impact[9]. Posterior observations also denied the 2036 impact [10], reassigning the value of 0 on the Torino scale to Apophis. Apophis is an Aten and Sq-type asteroid [11], based on its orbit and spectral type. Aten asteroids have Earth-crossing orbits with a semi-major axis of less than 1.0 AU (astronomical unit) and an aphelion greater than 0.983 AU. Sq asteroids have siliceous mineralogical compositions with the presence of metal. Apophis has an estimated bulk density of 3.19 g.cm^{-3}, as it resembles a LL ordinary chondrite [12], *i.e.*, a group of stony meteorites. A previous study already modelled the Apophis impact into the ocean and studied its consequences in detail [13].

Several studies address the impact of celestial bodies on Earth and its consequences. New algorithms to assess the paramount impact effects that might affect the population, infrastructure, and territory in the vicinity of an impact event were already published [14]. The algorithms estimate the asteroid's atmospheric passage, the cratering process, the thermal radiation emitted, the seismic shock intensity, the ejected material, and the severity of the air blast from airburst or surface impacts.

The virtual impacts of 315 asteroids included on NASA's

NEO risk list were assessed in [15]. This assessment included the impact location probability distribution. Later, the impact corridors for 261 observed asteroids that could impact the Earth before 2100 were reassessed [16]. Afterwards, the corridors were projected onto the Earth's map, considering the impact probability distributions. The cumulative impact probability distribution was paired with Earth's population to produce a risk map to recognise which nations are more prone to danger by an asteroid impact [17, 18, 19].

A software to assess the global impact risk of hazardous asteroids was developed and published [20]. It expresses the risk in terms of expected casualties and allows comparisons with other natural phenomena. The authors also derived and presented vulnerability models that associate the severity of impact effects with the human population.

As the Earth's surface is 71% water, the probability of a water impact is higher than a land impact. Therefore, the majority of future asteroid impacts on Earth should happen in marine environments. Water impacts generate two distinct tsunami waves, rim waves and collapse waves, which have little in common with the traditional earthquake-induced tsunami waves. Besides, a water depth of 6 – 8 times the diameter of a stony asteroid is enough to completely suppress the cratering process in the ocean floor [21].

The short-term regional consequences of asteroid impacts on the ocean were assessed in a similar case study [22], assuming the same impact location as the midpoint between Portugal's mainland, Azores, and Madeira Islands. The Apophis was one of the considered asteroids, along with a 204 m in diameter asteroid representative of the average impactor on the near-Earth objects, and a 5 km in diameter asteroid.

2. MODELLING

The authors followed a symbolic-numerical calculation to obtain the data for each point of interest while considering several premises to get more direct results. The impact was assumed to happen between mainland Portugal, Madeira, and the Azores, so no additional orbital mechanics calculations nor atmospheric entry assessments were required. The population was not warned about the threat, since it would be impossible to obtain the population vulnerability otherwise. Only direct effects were taken into account, so atmospheric, terrain, and wave reflections were not considered. As the impact was assumed to happen in deep waters, ground impact effects, such as seismic shaking and ejected material, were disregarded from the start.

The haversine formula, which determines the great-circle distance between two points on a sphere's surface, was used to obtain the distance from the impact site to the points of interest:

$$D = R_E \arccos\left[\sin\phi_i \sin\phi_k + \cos\phi_i \cos\phi_k \cos\left(|\lambda_i - \lambda_k|\right)\right] \tag{1}$$

where D is the distance to the impact site, R_E is the radius of the Earth, ϕ and λ are the latitude and longitude, and the coefficients i and k represent the impact location and the points of interest, respectively.

2.1. Cratering

The crater formation was an intricate process to model because it involves various stages, such as shock wave propagation, excavation of the impact surface, and depression formation, among others [14, 23]. However, as the impacts only happen in a liquid surface, only the transient crater dimensions were assessed. In [14, 20], through the usage of scaling laws and empirical data, analytical relations were developed to express the crater's dimensions. The transient crater diameter is given by:

$$D_{tc} = 1.365 \left(\frac{\rho_i}{\rho_t}\right)^{1/3} L^{0.78} v_i^{0.44} g_0^{-0.22} \sin^{1/3}\theta \tag{2}$$

where ρ_t and ρ_i are the densities of the target and the impactor, respectively; L is the impactor's diameter, v_i is the impact velocity, θ is the angle of impact, and g_0 is the Earth's standard gravitational acceleration.

The depth for the transient crater in relation the original ground plane was given by:

$$d_{tc} = \frac{D_{tc}}{2\sqrt{2}} \tag{3}$$

The volume of the transient crater was:

$$V_{tc} = \frac{\pi D_{tc}^3}{16\sqrt{2}} \tag{4}$$

2.2. Air Blast

Like explosions, a widely studied field, asteroid collisions generate shock waves that increase the atmospheric pressure at the vanguard [14, 25]. Th yield scaling distance D_1 that experiences the same peak overpressure as results from the explosion of 1 kt of TNT (trinitrotoluene, 1 TNT $= 4.184\times10^{12}$ J) can be found. The yield scaled distance D_1 is expressed as:

$$D_1 = \frac{D}{E_{kt}^{1/3}} \tag{5}$$

where D is the distance from the impact site and E_{kt} is the yield energy in kilotons TNT. The decay of the peak overpressure in Pa as a function of the yield scaled distance can be obtained by:

$$p_D = \frac{p_x D_x}{4D_1}\left(1 + 3\left[\frac{D_x}{D_1}\right]^{1.3}\right), \tag{6}$$

for which the values p_x and D_x were 75,000 Pa and 290 m, respectively, [14].

2.3. Thermal Radiation

In the vicinity of an impact site, the temperature and pressure are drastically raised[14, 26, 27]. A method that evaluates the thermal energy emanating from an impact event was presented in [14, 20]. For impact velocities higher than 12 km/s, the shock pressure could melt the impactor and some target material; vaporisation occurs for velocities higher than 15 km/s. The vapour generated, named the fireball, expands rapidly, and has very high pressure and temperatures. This thermal radiation model neglects the effects of atmospheric conditions and the variation in atmospheric absorption with altitude above the horizon. The relation between the radius of the fireball R_f in meters and the impact energy E in Joules is given by:

$$R_f = 0.002E^{1/3} \tag{7}$$

Thermal radiation is only a fraction of the kinetic energy released during an impact. This fraction, the luminous efficiency η_{lum}, for asteroid impacts with Earth is in the range of $10^{-4} - 10^{-2}$, a range found through limited experimental and numerical results in [14]. The thermal energy per area unit was given by:

$$\phi = f\frac{\eta_{lum}E}{2\pi D^2} \tag{8}$$

where f was the fraction of a fireball visible over the horizon at distance D, obtained by:

$$f = \frac{2}{\pi}\left(\cos^{-1}\frac{h}{R_f} - \frac{h}{R_f}\sin\left[\cos^{-1}\frac{h}{R_f}\right]\right) \tag{9}$$

In (9), h was the maximum height of the fireball below the horizon at a distance D, and it was defined by:

$$h = (1 - \cos\Delta)\, R_E \tag{10}$$

where Δ was the angle defined by:

$$\Delta = \arccos\left[\sin\phi_i \sin\phi_k + \cos\phi_i \cos\phi_k \cos\left(|\lambda_i - \lambda_k|\right)\right] \tag{11}$$

Then, using (7), if $h \geq R_f$, the fireball was entirely below the horizon, meaning that there was no direct thermal radiation reaching the location defined by (11), if the radiation deflection in the atmosphere is disregarded.

2.4. Tsunami

An asteroid impacting water creates a circular wave pattern, like a droplet impacting a liquid film. The event originates two types waves: rim waves and collapse waves. These waves could reach tremendous heights, hit inhabited coastal regions, and cause massive destruction. The assessment was divided into two stages: the deep-water wave amplitude propagation and the wave run-up in shallow waters. The wave amplitude attenuation models estimated the evolution of the maximum wave amplitude in waters deeper than 800 m, where the benthic strata depth was assumed to remain constant and equal to the impact location. In shallow waters, given the wave amplitude at the threshold point, the model estimated the run-up evolution until the coast, where a positive constant slope for the ocean floor was assumed.

2.4.1. Rim Wave

The initial asteroid impact on the ocean surface radially displaced the water to create the transient surface crater. This displacement originated the wave perturbation that eventually developed into the model's first tsunami wave, the rim wave. In [24], a propagation model was developed for the rim-wave amplitude. The models presented a $1/D$ wave decay with radial distance, which agreed with oceanic impact simulations [21]. The maximum rim-wave amplitude was:

$$A_{rw}^{max} = \min\left(\frac{D_{tc}}{14.1}, h_{sea}\right) \tag{12}$$

The rim-wave amplitude A_{rw} at a distance D from the impact location was:

$$A_{rw} = A_{rw}^{max}\left(\frac{3D_{tc}}{4D}\right) \tag{13}$$

2.4.2. Collapse Waves

The second type of wave is a product of the surface transient crater collapse. The impact-induced crater is filled by the adjacent ocean through centripetal inflow. The radial inflow creates a water peak at the centre of the then-collapsing crater that would continue to oscillate radially in and out until all energy is dissipated. Each oscillation generates a collapse wave. In the present model, the formation of the collapse wave is assumed to be unique and unrepeatable. In [24], a model to predict the collapse wave amplitude decay over the distance was defined. The maximum collapse wave amplitude was given by:

$$A_{cw}^{max} = 0.06\, min\left(\frac{D_{tc}}{2.828}, h_{sea}\right) \tag{14}$$

The collapse wave amplitude decay as a function of the distance D was defined as:

$$A_{cw} = A_{cw}^{max}\left(\frac{5D_{tc}}{2D}\right)^q \tag{15}$$

where q was the attenuation factor, defined as:

$$q = 3e^{-0.8L/h_{sea}} \text{ for } L/h_{sea} < 0.5 \tag{16}$$

2.4.3. Run-Up

The wave run-up U is the maximum height the wave can reach, i.e., the maximum vertical extent of a wave, given the slope s of the coastal region. In [20], a simple analytical model was developed to assess the run-up estimation U, which uses the following expression for its computation:

$$U = 2sA_{800}\left(\frac{A_{800}}{D_{tc}}\right)^{-0.5} \tag{17}$$

where A_{800} is the amplitude of the wave when it reaches shallow water, defined as being depths less than 800 m. The shore slope s is simply defined by the commonly known rise over run formula:

$$s = \frac{|h_{800} - h_k|}{D_{shore}} \tag{18}$$

where D_{shore} is the distance from the 800 m depth point to the location, h_{800} is per definition -800 m, and h_k is the location's altitude.

For every location, the maximum and minimum slopes were obtained by inserting the maximum $h_{k_{max}}$ and minimum $h_{k_{min}}$ altitude in (18). With these two new variables, the maximum run-up U_{max} and the minimum run-up U_{max} were assessed. However, even if the slope considers the elevation of the location, the run-up is in relation to the sea level. Thus, a local run-up U_l was determined which considers the minimum altitude of the location:

$$U_l = U - h_{k_{min}} \tag{19}$$

This local run-up could be defined with the minimum altitude resulting in the maximum local run-up, or on the other hand, with the maximum altitude resulting in the minimum run-up.

2.5. Global Effects

In [14], a simple way to assess the global effect was presented: computing the linear and angular momentum ratios between the Earth and the impactor, as well as the volume ratio of the transient crater diameter and the Earth's volume.

The linear momentum of the impactor M_i could be obtained by relating its mass m_i and its impact velocity v_i:

$$M_i = m_i v_i \tag{20}$$

Earth's linear momentum was obtained in a similar way while assuming its mass as $m_E = 5.83 \times 10^{24}$ kg and its mean orbital velocity as v_E = 29,780 m.s^{-1}. The angular momentum of the impactor was obtained by:

$$\Gamma_i = m_i v_i R_E \cos\theta. \tag{21}$$

The Earth's angular momentum was assumed to be Γ_E = 5.86 $\times$ 10^{33} kg.m^3.s^{-1}. The volume of the Earth was obtained assuming a 6371 km radius sphere. Depending on the three ratios mentioned, the qualitative global implications of the impact could be observed in Table 1.

Table 1: Global implications of an impact event [14]

Ratio	Interval	Qualitative global change
M_i/M_E	$]-\infty; 0.001[$	No noticeable change in orbit.
	$]0.001; 0.01[$	Noticeable change in orbit.
	$]0.01; 0.1[$	Substantial change in orbit.
	$]0.1; +\infty[$	Totally changes orbit.
Γ_i/Γ_E	$]-\infty; 0.01[$	No noticeable change in rotation period and tilt of axis.
	$]0.01; 0.1[$	Noticeable change in rotation period and tilt of axis.
	$]0.1; 1.0[$	Substantial change in rotation period and tilt of axis.
	$]1.0; +\infty[$	Totally changes rotation period and tilt of axis.
V_{tc}/V_E	$]-\infty; 0.1[$	Earth is not strongly disturbed and loses negligible mass.
	$]0.1; 0.5[$	Earth is strongly disrupted but loses a little mass.
	$]0.5; +\infty[$	Earth is completely disrupted and loses all mass.

The variation in the Earth's rotation period ΔT_E can be obtained using the asteroid's mass m_i, velocity v_i, and impact angle θ; and Earth's radius R_E, mass M_E, and rotation period T_E [24]:

$$\Delta T_E = \frac{5}{4\pi R_E}\frac{m_i}{M_E}\cos\theta\, v_i T_E^2 \tag{22}$$

2.6. Vulnerability

The vulnerability models estimate the population ratio lethally harmed by an asteroid impact. Vulnerability is intrinsically related to the severity of the impact effects, which is a function of the distance. Our models did not consider the time of day in which the impact event occurs, nor consider the terrain orography, the meteorological conditions, or the wind's direction. The populations were also assumed to have no previous warning about the threat. They were also independent of one another; i.e., the total vulnerability of a given location was not the sum of every individual effect's vulnerabilities.

2.6.1. Overpressure

High internal–external body pressure differentials endanger people. To extrapolate the vulnerability models, data that provided information about non-lethal, half-lethal, and completely lethal pressure differentials were utilised [28]. Best, worst, and expected pressure vulnerability models were developed with the bounding pressure values for each measure.

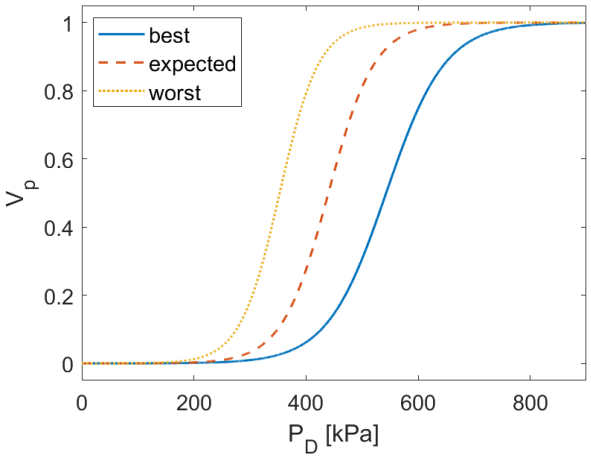

(a) Overpressure.

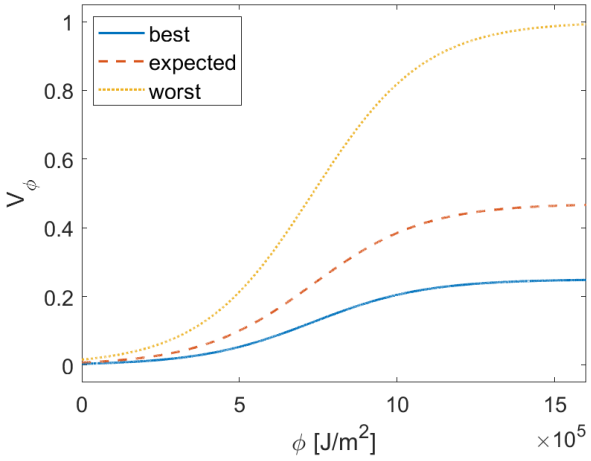

(b) Thermal radiation.

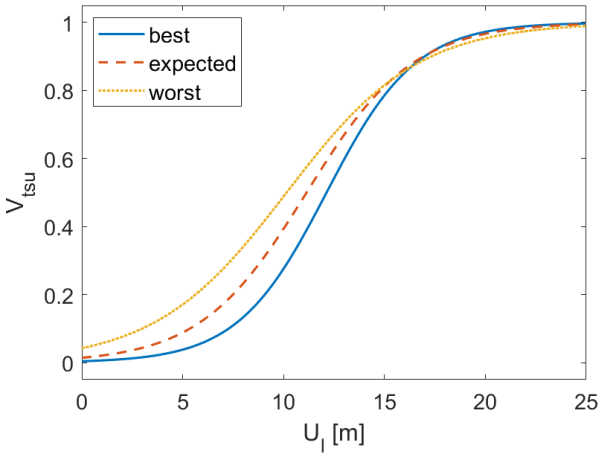

(c) Tsunami.

Fig. 1: Best, worst, and expected case vulnerability models.

However, these did not consider the potential effect on the population caused by damaged buildings. In Figure 1b, the vulnerability cases and the data are presented. The vulnerability models as logistic functions were as follows:

$$V_{\mathrm{p}} = \frac{1}{1 + e^{a(p+b)}} \tag{23}$$

Table 2: Overpressure vulnerability coefficients

	$a \times 10^5$	$b \times 10^{-5}$
best	-1.90	-5.43
expected	-2.42	-4.40
worst	-2.85	-3.53

The coefficients a and b are defined in Table 2. In Figure 1b, the three overpressure vulnerability scenarios are represented graphically.

2.6.2. Thermal Radiation

Thermal radiation could burn or ignite a surface that it encounters. This can include the skin, and therefore, thermal radiation could be fatal. In [28], different kinds of significant data were used to develop a thermal radiation vulnerability model. These data included the skin burn probability, the burn degree distribution as a function of the radiation exposure, and the mortality rates of treated and untreated burn victims as functions of burnt total body surface area. To obtain the mortality rate as a function of radiant exposure, the authors also considered that clothes offer some protection and that only one side of a person was exposed to radiation. Finally, to develop the different cases' vulnerability models, the authors considered the global unsheltered population at any given moment. For the best-case scenario, all the population was sheltered, but 25% were affected via windows. For the expected case, the unsheltered population is assumed to be 47%. In the worst-case scenario, all the population was assumed to be exposed. The vulnerability model was given by:

$$V_{\phi} = \frac{a}{1 + e^{b(\phi+c)}} \tag{24}$$

Table 3 presents the respective coefficients.

Table 3: Thermal radiation vulnerability coefficients

	a	$b \times 10^6$	$c \times 10^{-5}$
best	0.25	-5.62	-7.32
expected	0.47	-5.62	-7.32
worst	1.00	-5.62	-7.32

Figure 1c shows all three thermal exposure vulnerability models, the best, expected, and worst-case scenarios.

Table 4: Asteroids' physical and impact properties

	L [m]	θ [°]	ρ_i [kg/m^3]	v_i [m/s]	E [J]
2015 JJ	130	45	2600	15450	3.6×10^{17}
2020 FA_5	210	45	2600	29700	5.6×10^{18}
Apophis	375	45	3190	12620	7.0×10^{18}

2.6.3. Tsunami

A large body of water could be devastating when hitting an inhabited coastal region. The consequences of a tsunami is no easy task to assess as its highly complex and depends on various external factors. In [28], a simple analytical approach was developed to analyse a tsunami wave and its subsequent fatalities. The tsunami vulnerability was obtained as a function of the local run-up U_l, which varied according to the scenario, Table 5. The relation was:

$$V_{tsu} = \frac{1}{1 + e^{a(U_l + b)}}. \tag{25}$$

Its coefficients are defined in Table 5, and the visual representation is in Figure 1e.

Table 5: Tsunami vulnerability coefficients

	$a \times 10^1$	$b \times 10^{-1}$	U_l
best	-4.53	-1.21	$U_{min} - h_{k_{min}}$
expected	-3.80	-1.11	$(U_{min} + U_{max})/2 - h_{k_{min}}$
worst	-3.07	-1.02	$U_{max} - h_{k_{min}}$

3. RESULTS AND DISCUSSION

The midpoint between mainland Portugal, Azores, and Madeira had latitude and longitude of $39.6177°$ N and $16.9532°$ W, respectively, and was assumed as the impact location. As the impact effects depend heavily on the distance travelled by the impact effect, utilising single points to represent mainland Portugal, the Azores, and Madeira Islands is highly inaccurate. As such, the impact effects assessment was performed for all 308 Portuguese municipalities, considering each distance to the impact site. However, to not over-complicate the results exposition, the intensity of the impact effects is only shown for the closest municipality to the impact site on each of mainland Portugal, Azores, and Madeira. The casualties represent the individual municipality casualties' sums; e.g., the rim wave casualties attributed to Portugal represent the rim wave casualties of all Portuguese municipalities on the continent. The municipalities representatives of the three territories correspond to Peniche for mainland Portugal, Nordeste for Azores island, and Porto Santo for Madeira island. Table 4 displays the physical data of the three asteroids.

3.1. Cratering

The impacts occur on the water surface at a 45 degree angle with an impact velocity of v_i. The asteroids are assumed to be homogeneous spheres with diameters L and densities ρ_i. The transient crater diameter D_{tc} and depth d_{tc} of all impacts with the ocean surface were obtained via Equations (2)–(4), rather than modelling. The respective visual representations can be seen in Figure 2.

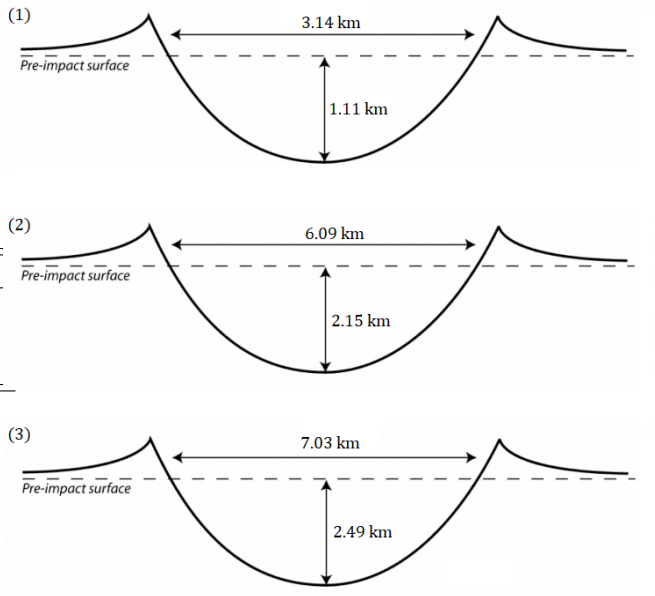

Fig. 2: Transient crater dimensions for the 2015 JJ (1), 2020 FA_5 (2), and Apophis (3) impacts.

3.2. Overpressure

The peak overpressure values from the impact-induced shock wave were obtained with (6). The distance D_1 in (5) is the distance to a 1 MT TNT equivalent explosion that experiences the same overpressure effects as the distance D from an impact energy E. Both the distance D_1 and the pressure P_D, for each impact scenario, are shown in Table 6. Figure 3 displays the peak overpressure P_D as a function of the distance D for the three asteroids.

The pressure values for the Apophis and 2020 FA_5 are in the high hundreds/low thousands, only potentially shatter-

Table 6: Impact effects in Portuguese territory

		D [km]	D_1 [km/kt$^{-1/3}$]	P_D [kPa]	h/R_f	ϕ [kJ/m^2]
2015 JJ	Portugal	650.3	14.8	0.375	23.4	0
	Azores	737.6	16.8	0.330	30.1	0
	Madeira	731.2	16.6	0.332	29.5	0
2020 FA$_5$	Portugal	650.3	5.91	0.974	9.36	0
	Azores	737.6	6.71	0.851	12.0	0
	Madeira	731.2	6.65	0.859	11.8	0
Apophis	Portugal	650.3	5.47	1.059	8.66	0
	Azores	737.6	6.21	0.925	11.1	0
	Madeira	731.2	6.16	0.933	10.9	0

ing windows, which requires 6.90 kPa. In the 2015 JJ scenario, the overpressure values lie in the low-hundreds range, not even allowing them to destroy windows.

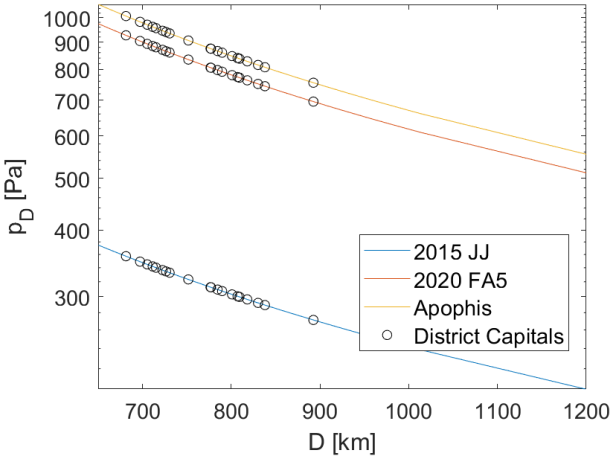

Fig. 3: Overpressure as functions of the municipalities' distances. The trends are represented by continuous lines.

3.3. Thermal Radiation

The thermal radiation assessment requires the estimation of the fireball, obtained with (7). Any other energy transfer method, such as atmospheric reflection, was dismissed. The influence of atmospheric conditions, as well as the atmospheric absorption variation with altitude was also disregarded. Because of the curvature of the Earth, two fractions related to the percentile of exposure of any location needed to be estimated to determine the radiation that reaches a given municipality. The first was the ratio between the maximum fireball height below the horizon and the fireball radius h/R_f. The second one was the fraction of visible fireball over the horizon f, defined in (9). Both are intrinsically related: if $h/R_f > 1$, then $f = 0$, and the municipality is completely shielded from direct exposure; if $0 < h/R_f < 1$, then $0 < f < 1$, meaning the location is exposed to thermal radiation, but has some protection; if $h/R_f = 0$, then $f = 1$, and the location is completely exposed, making Earth's curvature irrelevant. The luminous efficiency needs to be defined to complete the assessment and estimate the thermal radiation per location. This value is the fraction of kinetic energy converted into thermal radiation. We set the upper ϕ^+ and lower ϕ^- thermal radiation limits to 10^{-4} and 10^{-2} in the present work.

In Table 6, we can see the ratio of the maximum fireball height below the horizon to the radius of the fireball h/R_f, and the high and low thermal radiation bounds ϕ, for the Portuguese territory. For all impact scenarios, the h/R_f values surpass unity. All locations are shielded from direct exposure, thereby not experiencing thermal radiation. Since every location has a zero joule per square metre thermal exposure, the vulnerabilities and casualties associated with this impact effect are also zero.

3.4. Tsunami

The ocean depth at the impact location is 4.91 km. Thus, the ratio L_0/h_{sea} defines all the impacts as deep-water impacts, and the tsunami wave analysis consisted of two wave amplitude decay methods: one rim-wave amplitude method and one collapse wave amplitude method.

The wave amplitude propagation method assumes a constant ocean depth. The threshold between shallow and deep waters lies at the 800-m depth point, giving it extra significance [20]. Since the waters near the coast are less than 800 m deep and considered shallow, the amplitude method is not valid. Therefore, the authors employed a run-up wave computation method to properly assess the evolution of the waves near the coast and their final journey to the coastline. Figure 4 represents the tsunami waves amplitude at the threshold point obtained through (13) and (15). The red markers represent the values for the district capitals.The red markers represent the values for the district capitals.

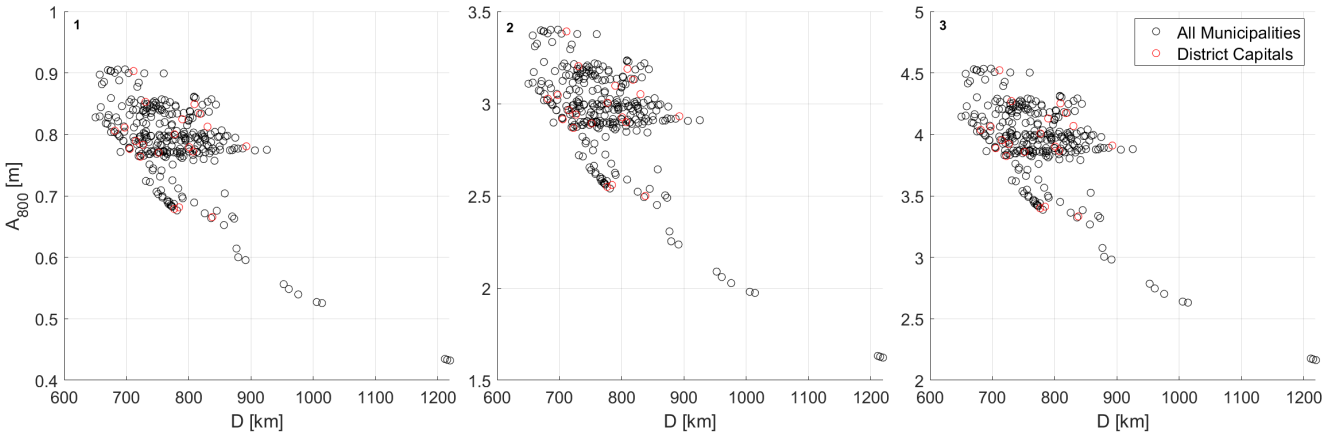

(a) Rim-wave amplitude.

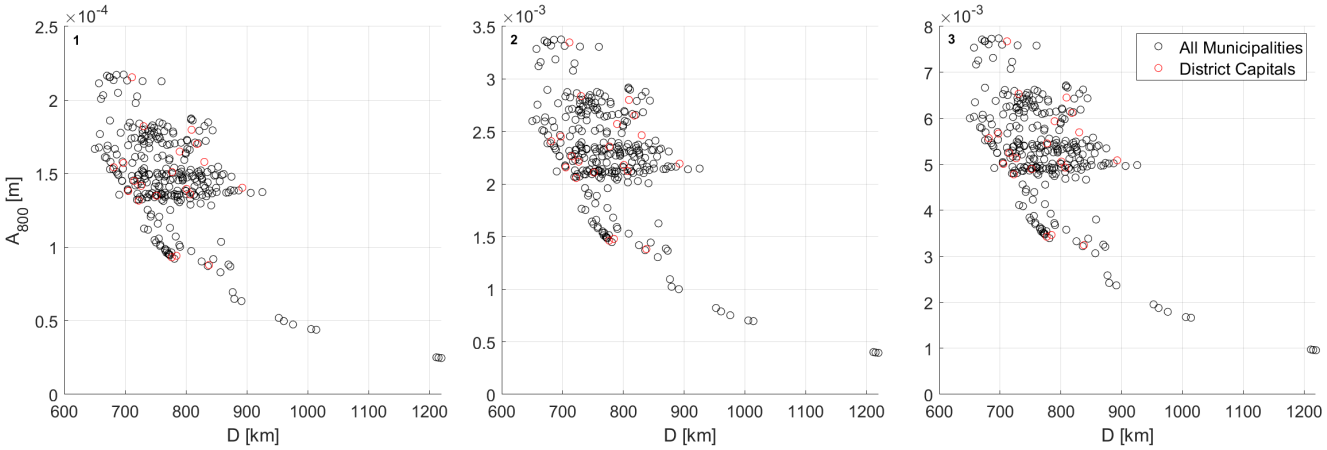

(b) Collapse wave amplitude.

Fig. 4: Tsunami wave amplitude, for the 2015 JJ (1), the 2020 FA_5 (2), and the Apophis (3), at the 800 m depth point as a function of the municipalities distance. The different marker's colour and shape represent all municipalities.

The main variable in the tsunami vulnerability assessment is the run-up wave at the coastline. Thus, the principal concern of the estimation is the wave behaviour in shallow water. To assess the run-up wave height, i.e., the height the wave can reach inland, the wave amplitude at the 800-m point A_{800} and the distance from this point to the shore D_{shore} are needed. The value obtained with (17) assumes the location in question is at sea level and cannot be directly used in the vulnerability models. Since most of the studied municipalities are not coastal, a local run-up was calculated considering the maximum and minimum altitude. PORDATA, a contemporary Portugal geography database [29], provided the needed altitudes. The EDMOnet grid, which presents a detailed bathymetry profile of the European seas [30], supplied the D_{shore} values.

In Table 7, the amplitude at the deep–shallow water threshold, along with the corresponding minimum and maximum run-up, are displayed for both waves. For the rim-wave assessment, the amplitude values entail few disparities among themselves. The values only diverge in the run-up assessment. From this observation, the impact energy dictates the absolute nature of the values considered: amplitude and run-up, and the different slopes dictate the run-up fluctuation. The Azores and Madeira Islands exhibit higher run-up values, possibly from their volcanic nature and the reduced continental shelf that protects the coast of mainland Portugal.

In Figures 5a and 6a, there is a side-by-side comparison of the minimum and maximum run-up that the rim-wave amplitude method generates for the three impacts. All these run-up values are in relation to the sea level. The altitude still needs to be considered to obtain the local run-ups. The red markers represent the values for the district capitals.

The second wave amplitude decay method, represented in (15), tries to model the wave amplitude attenuation of the collapse wave with the distance. Table 7 displays these amplitude values. The relation between the amplitude and run-up

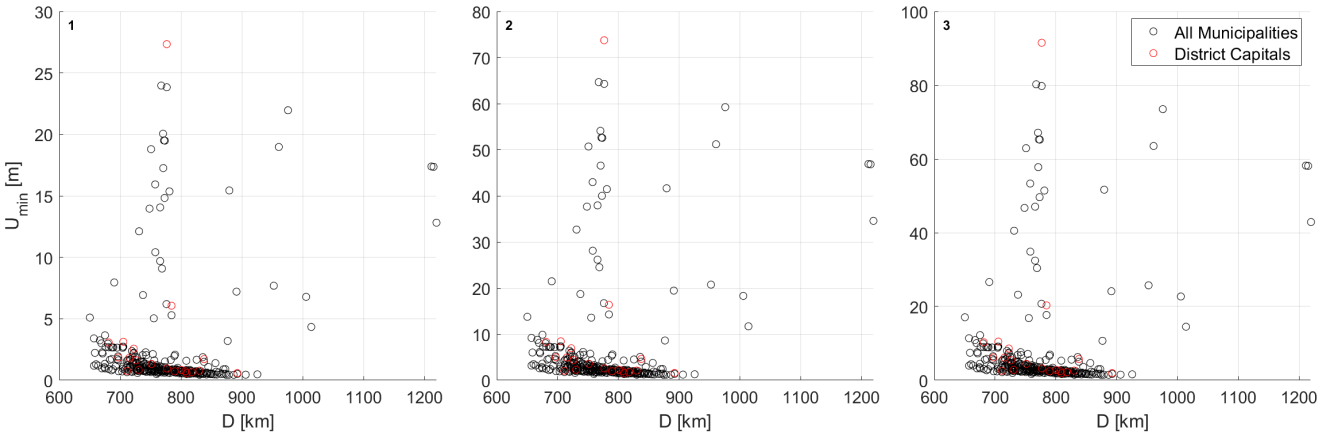

(a) Rim-wave.

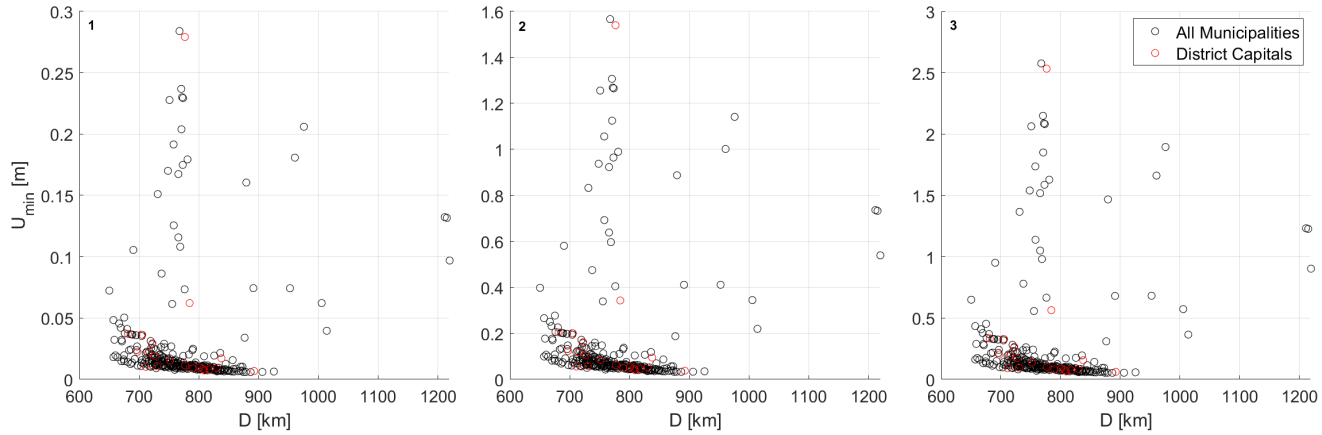

(b) Collapse wave.

Fig. 5: Tsunami wave minimum run-up, for the 2015 JJ (1), the 2020 FA_5 (2), and the Apophis (3), at the coast as a function of the municipalities' distance.

values is similar to that in the previously discussed model. However, for the collapse wave, the orders of magnitude of the amplitude and run-up are lower than in the rim-wave estimations.

The minimum and maximum run-up are represented in Figures 5b and 6b. The red markers represent the values for the district capitals. Most of the values are inferior to five metres, resulting in low vulnerability. The results show that a collapse wave is a lesser threat when compared to a rim wave.

3.5. Global Effects

Table 8 exposes the qualitative global implications of each impact studied. Row 1 represents the 2015 JJ impact; row 2 represents the 2020 FA_5 impact, and row 3 represents the Apophis impact. 2015 JJ would change the length of the day on Earth by 5 zeptosecond, which would be imperceptible by the population. The 202 FA_5 impact would change the length of the day on Earth by about 1 femtoseconds. The Apophis collision event would result in a 30 picosecond change in the total length of the day. The asteroids have relatively small diameters and do not cause any global change in the Earth's orbit, rotation period, tilt of the axis, or mass.

3.6. Vulnerability

This subsection displays the individual vulnerabilities and respective casualties for each impact effect. The vulnerabilities and casualties presented in this section are independent of one another. Thus, the total casualties from an impact are not the sum of the individual effects' casualties.

The overpressure vulnerability model is divided into three case scenarios: best, expected, and worst. Each scenario is associated with a specific overpressure vulnerability V_p and a subsequent casualties value C_p. Table 9 displays the air blast vulnerabilities and casualties. The overpressure causalities for the 2015 JJ, 2020 FA_5, and Apophis scenarios, rows 1, 2, and 3, respectively, despite reaching the hundreds on

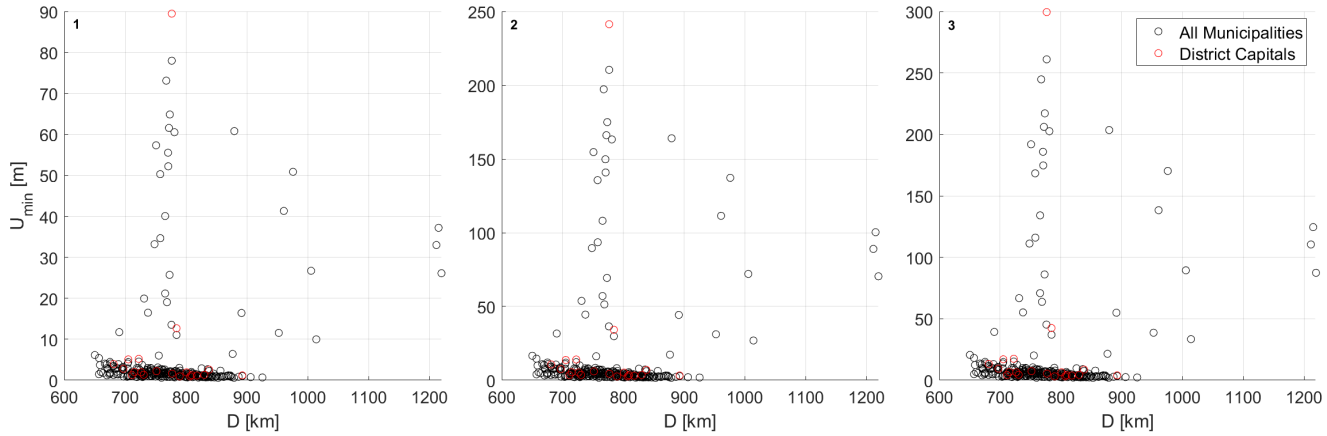

(a) Rim-wave.

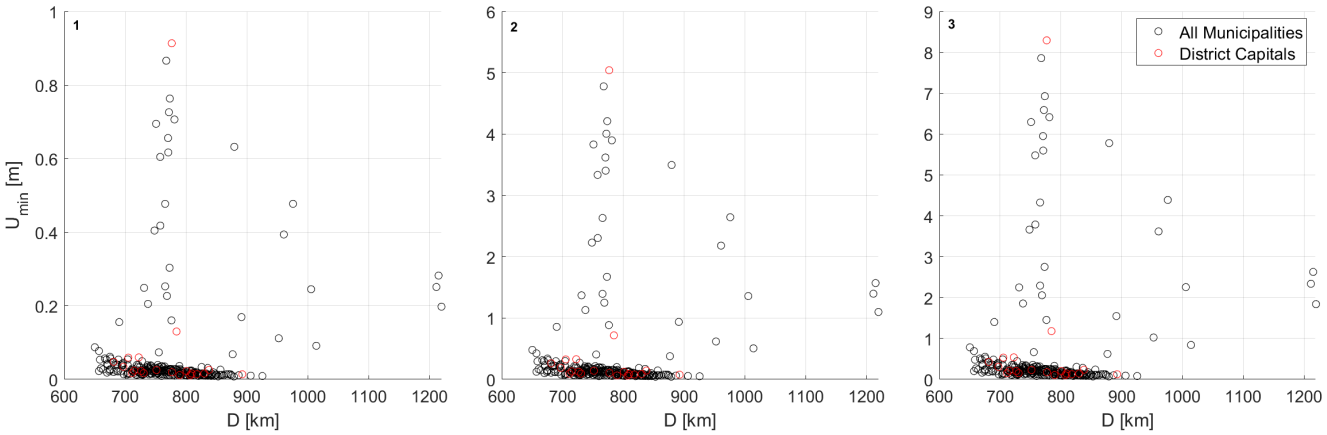

(b) Collapse wave.

Fig. 6: Tsunami wave maximum run-up, for the 2015 JJ (1), the 2020 FA_5 (2), and the Apophis (3), at the coast as a function of the municipalities' distance.

Table 7: Distance to the shore from the 800 m depth point, wave amplitude at this point and run-up heights, for the rim and collapse waves in Portuguese territory

			Rim-wave			Collapse wave		
		D_{shore} $[km]$	A_{800} $[m]$	U^- $[m]$	U^+ $[m]$	A_{800} $[mm]$	U^- $[m]$	U^+ $[m]$
2015 JJ	Portugal	16	0.828	5.10	6.15	0.167	0.072	0.087
	Azores	11	0.723	6.93	16.5	0.112	0.086	0.205
	Madeira	6.3	0.724	12.1	19.9	0.113	0.151	0.249
2020 FA_5	Portugal	16	3.11	13.8	16.6	2.60	0.398	0.480
	Azores	11	2.71	18.7	44.5	1.75	0.475	1.13
	Madeira	6.3	2.72	32.7	53.8	1.77	0.833	1.37
Apophis	Portugal	16	4.14	17.1	20.6	6.00	0.650	0.784
	Azores	11	3.62	23.2	55.2	4.09	0.780	1.86
	Madeira	6.3	3.63	40.6	66.8	4.12	1.37	2.25

Table 8: Global implications of the collision events

	Ratio	Value	Qualitative global change
	M_i/M_E	3×10^{-16}	No noticeable change in orbit.
1	Γ_i/Γ_E	4×10^{-14}	No noticeable change in rotation period and tilt of axis.
	V_{tc}/V_E	4×10^{-12}	Earth is not strongly disturbed and loses negligible mass.
	M_i/M_E	2×10^{-15}	No noticeable change in orbit.
2	Γ_i/Γ_E	3×10^{-13}	No noticeable change in rotation period and tilt of axis.
	V_{tc}/V_E	3×10^{-11}	Earth is not strongly disturbed and loses negligible mass.
	M_i/M_E	6×10^{-16}	No noticeable change in orbit.
3	Γ_i/Γ_E	9×10^{-13}	No noticeable change in rotation period and tilt of axis.
	V_{tc}/V_E	4×10^{-11}	Earth is not strongly disturbed and loses negligible mass.

Table 9: Overpressure vulnerabilities and casualties in Portuguese territory

		best		expected		worst	
		C_p	V_p $[10^{-5}]$	C_p	V_p $[10^{-5}]$	C_p	V_p $[10^{-5}]$
	Portugal	133	1.4	215	2.2	310	3.2
1	Azores	1	0.4	4	1.7	4	1.7
	Madeira	1	0.4	5	2.0	3	1.2
	Portugal	137	1.4	215	2.2	317	3.2
2	Azores	1	0.4	4	1.6	5	2.1
	Madeira	3	1.2	5	2.0	6	2.4
	Portugal	137	1.4	217	2.2	317	3.2
3	Azores	1	0.4	4	1.6	5	2.1
	Madeira	3	1.2	5	2.0	6	2.4

pascals, would not be significant when considering the entire Portuguese population.

The fireballs generated by the impacts would not be big enough to reach any of the studied locations. The vast distance between the impact site and each municipality would allow the curvature of the Earth to serve as a shield from direct thermal radiation. As every location would not be directly exposed to radiation, and this model does not consider radiation reflection or refraction, the vulnerabilities and respective casualties are considered to be zero.

Portugal is a geographically diverse country. It has coastal regions, exposed to the tsunami hazard, and mountain ranges, safer from such threats. The high altitudes of most municipalities are a natural defence from tsunami waves. However, Portugal's vast coast is completely exposed and exhibits considerable vulnerabilities. In Table 10 are displayed the vul-

Table 10: Rim-wave vulnerabilities and casualties in Portuguese territory

		best		expected		worst	
		C_{tsu}	V_{tsu}	C_{tsu}	V_{tsu}	C_{tsu}	V_{tsu}
	Portugal	6.24×10^4	0.006	2.10×10^5	0.022	5.37×10^5	0.055
1	Azores	4.45×10^4	0.184	1.20×10^5	0.495	1.77×10^5	0.729
	Madeira	2.36×10^5	0.929	2.54×10^5	0.997	2.54×10^5	0.999
	Portugal	4.12×10^5	0.042	1.04×10^6	0.106	1.83×10^6	0.187
2	Azores	1.94×10^5	0.802	2.34×10^5	0.963	2.40×10^5	0.990
	Madeira	2.54×10^5	1.000	2.54×10^5	1.000	2.54×10^5	1.000
	Portugal	7.26×10^5	0.074	1.60×10^6	0.163	2.43×10^6	0.248
3	Azores	2.19×10^5	0.904	2.39×10^5	0.987	2.42×10^5	0.997
	Madeira	2.54×10^5	1.000	2.54×10^5	1.000	2.54×10^5	1.000

Table 11: Collapse wave vulnerabilities and casualties in Portuguese territory

		best		expected		worst	
		C_{tsu}	V_{tsu}	C_{tsu}	V_{tsu}	C_{tsu}	V_{tsu}
1	Portugal	2.03×10^4	0.002	7.13×10^4	0.007	2.11×10^5	0.022
	Azores	1.02×10^3	0.004	3.66×10^3	0.015	1.09×10^4	0.045
	Madeira	1.16×10^3	0.005	4.39×10^3	0.017	1.35×10^4	0.053
2	Portugal	2.17×10^4	0.002	7.58×10^4	0.008	2.24×10^5	0.023
	Azores	1.22×10^3	0.005	4.68×10^3	0.019	1.43×10^4	0.059
	Madeira	1.91×10^3	0.008	1.91×10^3	0.041	3.59×10^4	0.141
3	Portugal	2.28×10^4	0.002	9.57×10^4	0.010	2.92×10^5	0.030
	Azores	1.42×10^3	0.006	5.79×10^3	0.024	1.81×10^4	0.075
	Madeira	2.84×10^3	0.011	2.00×10^4	0.079	7.05×10^4	0.278

nerabilities V_{tsu} and casualties C_{tsu} for the rim waves from the three impacts.

The rim wave casualties associated with the 2015 JJ asteroid are alarming. Considering a population of 2.42×10^5 for the Azores islands, in the best case, 18% of the population is affected, and in the worst case, the affected population could reach a value of 73% On Madeira Islands the scenario is even worst. The vulnerability ranges from 93% to 100%. For Portugal's mainland, considering a population of 9.78×10^6, the maximum vulnerability reaches 5.5% which still represents 5.37×10^5 people. The 2020 FA_5 rim wave generates alarming casualty numbers, especially considering that these numbers only represent coastal regions. The Madeira Islands, independent of the scenario, has casualties over 2.54×10^5. In mainland Portugal, the vulnerability ranges from 4.2% to 19%, which is still a significant threat, as those values correspond to 4.12×10^5 and 1.83×10^6 people. On the Azores Islands, the casualties range from over 1.94×10^5 to over 2.40×10^5. For the Apophis asteroid, the situation is very similar. For Portugal's mainland, in the best case, 7% of the population is affected by the rim wave, and in the worst-case scenario, the affected population could reach a value of 25%. The situation on the islands is even worse. For the Azores Islands, the rim wave affects 90% to 100% of the population. On Madeira Islands, all the 2.45×10^5 inhabitants are affected, independently of the scenario.

The vulnerabilities and casualties resulting from the collapse wave would be much lower; see Table 11. For the 2015 JJ asteroid, row 1, in mainland Portugal, the affected population ranges from 0.2% to 2.2%. However, 0.2% of the population is still 2.03×10^4, which is still alarming. In the Azores Islands, 4.5% is the maximum affected population, and in the Madeira Islands, in the worst scenario, 5.3% of inhabitants would be affected. Regarding the 2020 FA_5's results, row 2, the vulnerabilities of Portugal's mainland range from 0.2% to 2.3%, and for the Azores Islands, the vulnerabilities range from 0.5% to 5.9%. For Madeira Islands, in the worst-case scenario, the vulnerability reaches 14.1%. The Apophis scenario results in a maximum vulnerability of 3.0% for Portugal's mainland, 7.5% for Azores islands, and 28% for Madeira islands. Overall, the collapse wave is a lesser threat compared with the rim wave. However, the results on their own are still alarming. As the impact occurred in deep water in these scenarios, the results contradict previous statements [21] that collapse waves are the principal concern in deep oceanic impact events.

4. CONCLUSION

The current work studied the short-term regional consequences of three asteroid impacts on the Portuguese territory and population. The cosmic objects, assumed to impact the Earth at a $45°$ angle, included: the 2015 JJ asteroid, a 130-meter body, impacting the Earth with a velocity $v_i = 15.45$ km.s^{-1} and a density $\rho_i = 2600$ kg.m^{-3}; a 210 m asteroid, the 2020 FA_5, assumed to impact the Earth with a velocity $v_i = 29.70$ km.s^{-1} and a density $\rho_i = 2600$ kg.m^{-3}; and the 370 m Apophis asteroid, impacting the Earth with a velocity $v_i = 12.62$ km.s^{-1} and a density $\rho_i = 3190$ kg.m^{-3}. In addition to the impact assessment, the vulnerabilities and the casualties were assessed for each municipality and each impact effect independently.

Each impact effects assessment included a shock wave, thermal radiation, tsunami waves, and the qualitative global effects. For all impacts, the average pressure difference experienced in Portuguese territory because of the shock wave could only potential shatter windows. The fireball is not big enough to endanger the municipalities. The tsunami would be felt throughout the coastal territory in all three impact events, making it the most concerning impact effect. Regarding global implications, no impact was on a scale big enough to affect the Earth's orbit, rotation period, rotational axis, or mass.

The vulnerability was assessed through pre-established vulnerability models for all the impact effects studied. All the models were subdivided into three case scenarios: best,

expected, and worst.

The final estimates were of casualties in every municipality for every impact effect. There was a direct correlation between asteroid impact risk and population density. As such, the casualties were assessed with a simple product relation between the vulnerability and the population count.

The rim wave was the most hazardous impact effect for all three impacts, having the highest average vulnerability values. The tsunami wave, independently of the scenario considered, had the ability to destructively affect several hundred-thousand or several million Portuguese people.

Acknowledgements

The present work was performed under the scope of activities at the Aeronautics and Astronautics Research Center (AEROG) of the Laboratório Associado em Energia, Transportes e Aeronáutica (LAETA), and was supported by the Fundação para a Ciência e Tecnologia by Project No. UIDB/50022/2020.

5. REFERENCES

[1] Jet Propulsion Laboratory, "JPL Small-Body Database Browser: (2015 JJ)," [Online]. Available: https://ssd.jpl.nasa.gov/tools/sbdb_lookup.html#/?sstr=2015%20JJ, [Accessed: 17-May-2022].

[2] NASA/JPL: Near-Earth Object Program Office, "Earth Impact Risk Summary: 2015 JJ," [Online]. Available: https://cneos.jpl.nasa.gov/sentry/details.html#?des=2015%20JJ, [Accessed: 17-May-2022].

[3] Jet Propulsion Laboratory, "JPL Small-Body Database Browser: (2020 FA_5)," [Online]. Available: https://ssd.jpl.nasa.gov/tools/sbdb_lookup.html#/?sstr=2020%20FA5, [Accessed: 17-May-2022].

[4] NASA/JPL: Near-Earth Object Program Office, "Earth Impact Risk Summary: 2020 FA_5," [Online]. Available: https://cneos.jpl.nasa.gov/sentry/details.html#?des=2020%20FA5, [Accessed: 17-May-2022].

[5] T. G. Müller, C. Kiss, P. Scheirich, P. Pravec, L. O'Rourke, E. Vilenius, and B. Altieri, "Thermal infrared observations of asteroid (99942) Apophis with Herschel," *Astronomy and Astrophysics*, vol. 566, pp. 1–10, 2014.

[6] J. Licandro, T. Müller, C. Alvarez, V. Alí-Lagoa, and M. Delbo, "GTC/CanariCam observations of (99942) Apophis," *Astronomy and Astrophysics*, vol. 585, pp. 1–4, 2016.

[7] Steven R. Chesley, "Potential impact detection for near-Earth asteroids: The case of 99942 Apophis (2004 MN4)," *Proceedings of the International Astronomical Union*, vol. 1, no. S229, pp. 215–228, 2005.

[8] Jon D. Giorgini, Lance A.M. Benner, Steven J. Ostro, Michael C. Nolan, and Michael W. Busch, "Predicting the Earth encounters of (99942) Apophis," *Icarus*, vol. 193, no. 1, pp. 1–19, 2008.

[9] D. Farnocchia, S. R. Chesley, P. W. Chodas, M. Micheli, D. J. Tholen, A. Milani, G. T. Elliott, and F. Bernardi, "Yarkovsky-driven impact risk analysis for asteroid (99942) Apophis," *Icarus*, vol. 224, no. 1, pp. 192–200, 2013.

[10] Peng Guo, V. V. Ivashkin, C. A. Stikhno, and P. M. Shkapov, "Determination and investigation of asteroid Apophis' trajectories set potentially colliding with the Earth in 2036," *IOP Conference Series: Materials Science and Engineering*, vol. 468, no. 1, 2018.

[11] Richard P. Binzel, Andrew S. Rivkin, Cristina A. Thomas, Pierre Vernazza, Thomas H. Burbine, Francesca E. DeMeo, Schelte J. Bus, Alan T. Tokunaga, and Mirel Birlan, "Spectral properties and composition of potentially hazardous Asteroid (99942) Apophis," *Icarus*, vol. 200, no. 2, pp. 480–485, 2009.

[12] D. T. Britt, D. Yeomans, K. Housen, and G Consolmagno, "Asteroids Density, Porosity, and Structure," in *Asteroids III*, W. Bottke, A. Cellino, P. Paolicchi, and R.P. Binzel, Eds., chapter 4.2, pp. 485—-500. University of Arizona Press, Tucson, AZ, USA, 2002.

[13] Renato H. Morais, Luís F.F.M. Santos, André R.R. Silva, and Rui Melicio, "Hypothetical Apophis deep ocean impact—Energy analysis," *Acta Astronautica*, vol. 188, pp. 438–450, 2021.

[14] Gareth S. Collins, H. Jay Melosh, and Robert A. Marcus, "Earth Impact Effects Program: A Web-based computer program for calculating the regional environmental consequences of a meteoroid impact on Earth," *Meteoritics and Planetary Science*, vol. 40, no. 6, pp. 817–840, 2005.

[15] Clemens M. Rumpf, "Global Asteroid Risk Analysis," in *International Astronautical Congress 2014 - "Move An Asteroid"*, Toronto, Canada, 2014, pp. 1–10.

[16] Clemens M. Rumpf, Hugh G. Lewis, and Peter M. Atkinson, "GLOBAL IMPACT DISTRIBUTION OF ASTEROIDS AND AFFECTED POPULATION," in *4th IAA Planetary Defense Conference*, 13-17 April 2015, Frascati, Roma, Italy, 2015, pp. 1–9.

[17] Clemens M. Rumpf, Hugh G. Lewis, and Peter M. Atkinson, "Monitoring the Global Asteroid Impact Risk," in *66th IAF International Astronautical Congress*, Jerusalem, Israel, 2015, pp. 1–12.

[18] Clemens M. Rumpf, Hugh G. Lewis, and Peter M. Atkinson, "The global impact distribution of Near-Earth objects," *Icarus*, vol. 265, pp. 209–217, 2016.

[19] Clemens M. Rumpf, Hugh G. Lewis, and Peter M. Atkinson, "On the influence of impact effect modelling for global asteroid impact risk distribution," *Acta Astronautica*, vol. 123, pp. 165–170, 2016.

[20] Clemens M. Rumpf, *Asteroid Impact Risk*, Ph.D. thesis, University of Southampton, Southampton, UK, 2016.

[21] K. Wünnemann, G. S. Collins, and R. Weiss, "Impact of a cosmic body into Earth's Ocean and the generation of large tsunami waves: Insight from numerical modeling," *Reviews of Geophysics*, vol. 48, no. 4, pp. 1–26, 2010.

[22] Renato H. Morais, Luís F. F. M. Santos, André R. R. Silva, and Rui Melicio, "Short-term consequences of asteroid impacts into the ocean: A portuguese case study," *Universe*, vol. 8, no. 5, 2022.

[23] Brandon C. Johnson, Gareth S. Collins, David A. Minton, Timothy J. Bowling, Bruce M. Simonson, and Maria T. Zuber, "Spherule layers, crater scaling laws, and the population of ancient terrestrial impactors," *Icarus*, vol. 271, pp. 350–359, 2016.

[24] Gareth Collins and Jay Melosh, "Errata and Improvements in Earth Impact Effects Program," 2013.

[25] Gareth S. Collins, Elliot Lynch, Ronan McAdam, and Thomas M. Davison, "A numerical assessment of simple airblast models of impact airbursts," *Meteoritics and Planetary Science*, vol. 52, no. 8, 2017.

[26] V. V. Svetsov and V. V. Shuvalov, "Thermal radiation and luminous efficiency of superbolides," *Earth and Planetary Science Letters*, vol. 503, pp. 10–16, 2018.

[27] Vladimir Svetsov and Valery Shuvalov, "Thermal radiation from impact plumes," *Meteoritics and Planetary Science*, vol. 54, no. 1, pp. 126–141, 2019.

[28] Clemens M. Rumpf, Hugh G. Lewis, and Peter M. Atkinson, "Population vulnerability models for asteroid impact risk assessment," *Meteoritics and Planetary Science*, vol. 52, no. 6, pp. 1082–1102, 2017.

[29] PORDATA, "Base de Dados de Portugal Comtemporâneo," [Online]. Available: `https://www.pordata.pt/Municipios/Altitude+m%c3%a1xima-50` & `https://www.pordata.pt/Municipios/Altitude+m%c3%adnima-49`, [Accessed: 30-Apr-2020].

[30] EMODnet, "Undersanding the topography of the European seas," [Online]. Available: `https://portal.emodnet-bathymetry.eu/`, [Accessed: 04-May-2020].